Spectrochimica Acta Part A: Molecular and Biomolecular Spectroscopy 285 (2023) 121903

Contents lists available at ScienceDirect

Spectrochimica Acta Part A:
Molecular and Biomolecular Spectroscopy

journal homepage: www.journals.elsevier.com/spectrochimica-acta-part-a-molecular-and-biomolecular-spectroscopy

Surface-enhanced Raman spectral characterization of antifungal activity of selenium and zinc based organometallic compounds

Ali Raza [a], Soneya Parveen [b], Muhammad Irfan Majeed [a,*], Haq Nawaz [a,*], Muhammad Rizwan Javed [c], Muhammad Adnan Iqbal [a], Nosheen Rashid [d], Muhammad Zeeshan Haider [a], Muhammad Zeeshan Ali [a], Amina Sabir [a], Hafiz Mahmood ul Hasan [a], Beenish Majeed [a]

[a] Department of Chemistry, University of Agriculture Faisalabad, Faisalabad 38000, Pakistan
[b] Medicine and Allied, Faisalabad Medical University, Faisalabad 38000, Pakistan
[c] Department of Bioinformatics and Biotechnology, Government College University Faisalabad (GCUF), Faisalabad 38000, Pakistan
[d] Department of Chemistry, University of Education, Faisalabad Campus, Faisalabad 38000, Pakistan

HIGHLIGHTS

- SERS is employed to evaluate antifungal activity of Zinc and selenium organometallic compounds.
- Silver nanoparticles are used as SERS substrates.
- SERS spectral features are associated in comparison with different ligands and their respective ligands.
- Principal components analysis (PCA) is found helpful for the differentiation between SERS spectral data of silver and zinc NHC complex exposed *A. niger* and unexposed control fungus.
- PLSDA model is validated and can be used for the classification of Se-NHC and Zn-NHC complexes.

GRAPHICAL ABSTRACT

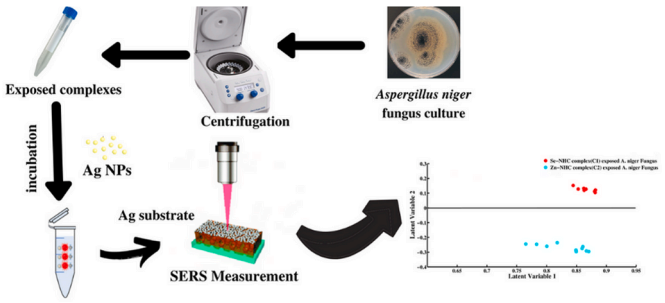

ARTICLE INFO

Keywords:
Aspergillus niger
Antifungal activity
Se-NHC complexes
Surface-enhanced Raman spectroscopy
Partial least square discriminant analysis

ABSTRACT

Surface-enhanced Raman spectroscopy (SERS) is used to identify the biochemical changes associated with the antifungal activities of selenium and zinc organometallic complexes against *Aspergillus niger* fungus. These biochemical changes identified in the form of SERS peaks can help to understand the mechanism of action of these antifungal agents which is important for development of new antifungal drugs. The SERS spectral changes indicate the denaturation and conformational changes of proteins and fungal cell wall decomposition in complex exposed fungal samples. The SERS spectra of these organometallic complexes exposed fungi are analyzed by using statistical tools like principal component analysis (PCA) and partial least square discriminant analysis (PLS-DA). PCA is employed to differentiate the SERS spectra of fungal samples exposed to ligands and complexes. The PLS-DA discriminated different groups of spectra with 99.8% sensitivity, 100% specificity, 98% accuracy and 86 % area under receiver operating characteristic (AUROC) curve.

* Corresponding authors.
E-mail addresses: irfan.majeed@uaf.edu.pk (M.I. Majeed), haqchemist@yahoo.com (H. Nawaz).

https://doi.org/10.1016/j.saa.2022.121903
Received 27 May 2022; Received in revised form 14 September 2022; Accepted 15 September 2022
Available online 20 September 2022

1. Introduction

Antifungal drugs are playing a very important role in human health care by treating fungal infections as well as by preventing their further spread inside the body [1]. Organometallic compounds are employed to cure resistive fungal infections, which are hazardous to human health and the mortality rate of Invasive Fungal infections IFI (1,660,000) is greater than malaria (445,000) and equivalent to tuberculosis (1,700,000) [2]. Antimicrobial drugs are necessary during surgical or medical procedure, organ transplant, chemotherapy, etc. [3]. However, fungus have an ability to induce resistance against the drugs after prolong usage and hence the newer drugs with better inhibition ability are usually require [4].

Antifungal activity of the organometallic compounds is an attractive approach to find new drug candidates against pathogens [5]. N-heterocyclic carbene complexes are utilized as pharmaceutical agents for cancer therapy, antimicrobial, antioxidant, anti-inflammatory, and antifungal activities because of their various physiological functions [6]. Selenium is a biocompatible micronutrient due to its low toxicity toward humans, therefore its complexes containing carbene release selenium to the biological system which acts as an effective pharmaceutical agent. In medicinal chemistry, selenium can cure many kinds of diseases due to its compatibility with human body including cancer, Alzheimer's, oxidative stress, Human immunodeficiency virus HIV, and depression [7,8].

Currently, many drugs of metal complexes are routinely administered to patients for therapeutic purposes [9]. It has been explored that the metal-based antimicrobial agents play a better role against the bacteria and may act as future antimicrobial drugs [10]. Similarly, selenium metal based organometallic complexes are being applied as pharmacological agents such as anticancer activities [8], antioxidant activities [11], antimicrobial activities [12], anti-inflammatory activities [13].

The antifungal assays for different drug candidates are performed by radial growth inhibition, which is used to detect the Minimum inhibition concentration (MIC) values of compounds to check the ability of drugs as antifungal agents [14]. These assays are much laborious, tedious and expensive. Therefore, new methods should be developed which are non-invasive, require less consumables and rapid [15].

Raman spectroscopy is employed for several applications in pharmaceutical drugs to study the active pharmaceutical ingredient [16]. Raman spectroscopy is considered a technique of choice for analyzing drug-target interaction [17] and interaction of drug candidates with the bacteria and fungi [18]. Surface enhanced Raman spectroscopy is the modality in this field offering high signal to noise ratio. SERS can be utilized to get Raman spectral information from complex bio systems rapidly and at high lateral resolution [19]. SERS play important rule in biological systems and biomedical media. Recent advancement in fields of SERS include a novel ultrasensitive and universal "Raman indicator" sensing strategy proposed for protein detection [20] and molecular imprinting [21,22]. Gold NPs are well known for their stability and preferred choice when a matter of chemical inertness is required but silver is choice as SERS substrate for the greater enhancement when irradiated with 785 nm laser for the analysis of biological materials [23]. Recent studies have shown an impressive potential of Ag-NPs as SERS substrates for diagnostic applications [24]. Moreover, Ag NPs are considered as candidates for SERS because of ease of preparation and providing more active sites which ultimately lead to the stronger SERS enhancement factor [25]. Water dilution of nanoparticles was controlled by keeping the solution concentrated. It is reported that in very dilute solution only 12% Ag NPs particles dissolve in water after 17 days [26] {Loza, 2014 #47}. In the current study, freshly prepared Ag-NPs were used and SERS spectra were acquired in a single day to overcome the problems associated with their stability and water solubility.

In present study, fungal strain, *Aspergillus Niger* (*A. Niger*) is exposed to organometallic compounds of selenium and zinc and subjected for SERS analysis in comparison with unexposed/control *A. Niger* fungus.

The SERS features of unexposed/control and exposed A. *Niger* are analyzed by using comparison of respective mean spectra and principal components analysis (PCA). The differentiating SERS features can be identified in the spectra of unexposed/control as compared to fungus exposed to selenium complex. The differentiating SERS features can be identified in the spectra of unexposed/control as compared to fungus exposed to selenium and zinc complexes. This spectral information may help to understand the biochemical changes taking place due to the action of two different complexes on fungus and leads to identify the mode of action of these potential antimicrobial agents.

2. Materials and methods

2.1. Antifungal screening

Agar well diffusion method was used to check the antifungal activities of different concentrations of ligands and their respective selenium and zinc complexes against fungal pathogens. In this method 1 mL of fresh fungal culture was dropped in the center of sterile Petri plate along with molten cooled muller containing the inoculum and mixed well. After the solidification of plate its inoculum wells were filled with the 100 μl of each concentration of antifungal compound and 10% DMSO was employed as negative control. These plates were then incubated at 37 °C for 18 h for testing the antifungal activity of different concentrations of each compound against A. *niger* fungal strain. Zone of inhibition (including the wells diameter) was measured for demonstrating the antifungal activity of different concentrations of each compound. Minimum inhibitory concentrations (MICs) of the ligands and their respective Selenium and Zinc complexes were determined against *A. niger*. It was found that 80% concentration (MIC) of Selenium and zinc complex show greater inhibition for A. niger fungal strain as compared with their ligands. However, these exposed fungal strain samples were subjected for Surface enhanced Raman spectroscopic analysis (SERS).

2.2. Synthesis of nanoparticles

The silver nanoparticles were synthesized by the process described by Leopold and Lendel [27]. For that 17 mg of silver nitrate was dissolved in 10 mL of deionized water (Milli Q). The morphology and the size of Ag-NPs was determined by using the SEM, TEM and UV–visible spectrometer. The greenish Ag suspension was kept at 4 °C in dark for further use.

The Ag-NPs were characterized with field emission electron microscope (FEM) (JEOL, JSM-7500F). FEM operates in both modes as scanning and transmission electron microscope (FESEM and FETEM) with a 30 KeV operating voltage. For TEM analysis, samples were prepared by slow evaporation of a drop of aqueous suspension of Ag-NPs on carbon coated copper grid (400 mesh), while SEM samples were prepared by simply placing nanoparticles on sample holder without any extra conductive coating. The ImageJ software was used for analyzing the electron micrographs and size of prepared Ag-NPs was determined.

2.3. Acquisition of SERS spectra

Raman spectra of samples were acquired by Raman spectrometer (Peak Seeker Pro-785; Agiltron, USA). A fraction of each sample was put on the aluminum slide and Raman spectra were recorded by using 785 nm laser with the help of 40X objective. For this purpose, wavelength range was 600–1800 nm and 15 Raman spectra of each fungal sample were collected with acquisition time of 10 s.

2.4. Data preprocessing

SERS spectral data preprocessing was performed with in house-built codes of MATLAB 7.8 [28] includes smoothening, baseline correction, vector normalization and substrate removal. SERS data was smoothed

with Savitzky-Golay smoothing method and spectral baseline was corrected with rubber band and polynomial algorithms. The spectra of substrate (Aluminum loaded with Ag-NPs) were removed from SERS spectra of all the samples.

2.5. Data analysis

SERS spectral data was analyzed by using chemometric technique, principal component analysis (PCA) and partial least square discriminant analysis (PLS-DA). PCA technique transforms correlated variables into smaller sets of uncorrelated variables that are called principal components (PCs). PCA uses principal components (PCs) for differentiating different spectral data sets and it helps in reducing dimensionality of data set by maintaining variance. The PC1 explains maximum variance while successive PCs are used for explaining remaining variance in data set. PLS-DA as a multivariate data mode was performed by using the unexposed/exposed (class information) as **y**-variable and spectral data as **x**-variable. The cross-validation was used along it to find out the optimal number of latent variables (LVs). The data obtained was used for classifying the spectral data of Se-NHC, Zn-NHC complex exposed *A. Niger* fungus from unexposed ones. The performance and efficacy of the model was determined by calculating the specificity, sensitivity, accuracy and the Receiver operating curve approach.

3. Results and discussion

The Ag-NPs were characterized by using scanning electron microscope (SEM) and transmission electron microscope (TEM). The scanning electron microscopy (SEM) and transmission electron microscopy (TEM) images of silver nano particles are shown in supplementary material Fig. S-1. Silver nanoparticles have received great attention due to their physical and chemical properties. Absorption and scattering properties of silver nanoparticles change by controlling the particle size shape and refractive index near the particle size. Moderately large nanoparticles have good enhancement as compared with smaller nanoparticles [29]. The roughened surface of silver nano particles shows the stronger Raman enhancement. The NPs were found to be spherical in geometry with average size of 65 × 45 nm as described in supplementary material, Fig. S1. The nanoparticles of this geometry and size were previously used for SERS activities and showed good enhancement of SERS signals [30,31].

Fig. 1 shows SRES spectra of ligand exposed A. niger **(L1)**, complex exposed A.niger **(C1;** Se-NHC complex**)** and unexposed/control A. niger. SERS signal provided by this screening method presented, though weak but reproducible and reliable results, therefor these are reported as discriminating SERS features among the unexposed and exposed fungal strains. The SERS spectral features which are associated with the biochemical changes taking place in the fungus after ligand and complex exposure as compared with unexposed/control include 592 cm^{-1} (υ(C–C–C) of cell wall component), 650 cm^{-1} (C–S stretch and C–C twist (Protein)), 674 cm^{-1} (Glycosidic ring breathing mode), 734 cm^{-1} (hypoxanthine), 784 cm^{-1} (nucleic acids (cytidine, uracil)), 765 cm^{-1} (O-P-O DNA), 768 cm^{-1} (Hydroxyl radical), 823 cm^{-1} (O-P-O DNA), 878 cm^{-1} (O–O stretch (H_2O_2)), 929 cm^{-1} (R-CH_3 of valine), 959 cm^{-1} (C–C–N stretch (protein)), 1006 cm^{-1} (S–O, stretching (phenylalanine)), 1032 cm^{-1} (O-P-O DNA), 1054 cm^{-1} (C-N stretching (protein)), 1098 cm^{-1} (CC skeletal and COC str from glycosidic link), 1416 cm^{-1} (=C-C=unsaturated fatty acids (lipid)), 1191 cm^{-1} (Guanine), 1210 cm^{-1} (Amide III of proteins), 1239 cm^{-1} (Amide III and Amide I of proteins),1328 cm^{-1} (υ (NH_2) adenine, polyadenine, DNA), 1375 cm^{-1} (hypoxanthine), 1460 cm^{-1} (CH_2 lipid), 1469 cm^{-1} (Adenine and Guanine), 1420–1480 cm^{-1} (CH deformation mode (protein)), 1515 cm^{-1} (Cytosine), 1103 cm^{-1} (Phenylalanine), 1604 cm^{-1} (Amide I), 1610 cm^{-1} (tryptophan) (see Table 1).

Some SERS spectral features which are directly related with DNA/RNA contents include 784 cm^{-1} (nucleic acids (cytosine, uracil)), 1328 cm^{-1} (υ (NH_2) adenine, polyadenine, DNA), 1469 cm^{-1} (Adenine and Guanine) and their intensities are continously decreasing from ligand to complex as compared with unexposed/control. It is observed that decreases in the intensities of theses SERS spectral features are related with degardion of DNA/RNA contents of fungus in complex exposed fungal samples as compared with ligand and unexposed/control sample. Similary, SERS features at 734 cm^{-1} (hypoxanthine), 784 cm^{-1} (cytosine and uracil bases) and 1191 cm^{-1} (Guanine) are also associated with destruction of fungal DNA molecule because hypoxanthine is fragmented product of fungal DNA [32].

Some SERS specrtral festures which are dirctly associated with protein contents of fungus including 650 cm^{-1} (C–S stretch and C–C twist), 823 cm^{-1} (O-P-O DNA), 929 cm^{-1} (R-CH_3 of valine protein band), 959 cm^{-1} (C–C–N stretch (protein)), 110 Phenylalanine (proteins) and 1208 cm^{-1} (Guanine) their intensities are continously decreasing from ligand to complex as compared with unexposed/control one. This reduction in peak intensities are directly related with denaturation and conformational changes of proteins in complex exposed fungal samples as compared with ligand and unexposed/control fungal samples [33].

The SERS spectral features with reducing intensities at 575 cm^{-1} (Glycosidic ring mode), 565 cm^{-1} (C–C str), 765 cm^{-1} (O-P-O DNA) are associated with inhibition of β-1, 3-glucan synthase in fungus cell wall. These reducing SERS spectral features are directly related with the degradation of fungal peptidoglycane in complex exposed fungal

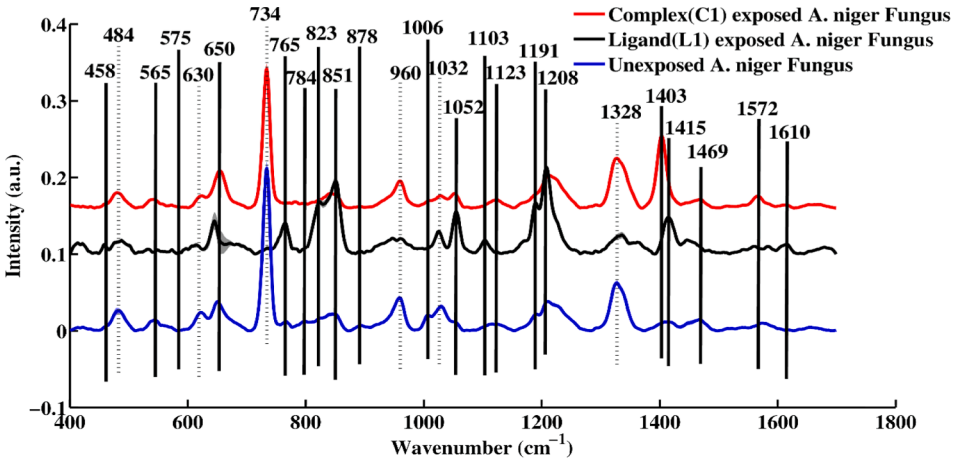

Fig. 1. The SRES spectra of ligand exposed A. niger **(L1)**, complex exposed A.niger **(C1)** and unexposed/control A. niger **(C)**. SERS spectral data along with potenially differentiating features are labelled with solid and dotted lines and are listed in Table 1.

Table 1
SERS spectral features of ligands and their respective Se and Zn-NHC complexes.

Wavenumber (cm^{-1})	SERS Peak Assignment	Components	References
546	Ring def	Carbohydrates	[42]
565	β(C˙C˙O)	Carbohydrates	[43]
575	Glycosidic ring mode	Carbohydrates	[44]
592	β(C˙C˙C), ring def	Carbohydrates	[36]
630	υ(O–C=O) of oxalic acid)	Proteins	[37]
650	C–S stretch and C–C twist	Proteins	[37]
674	A ring breathing mode of DNA and RNA bases	Carbohydrates	[32]
734	The ring breathing mode from hypoxanthine, adenine, adenosine,	DNA/RNA	[45]
765	O-P-O DNA	DNA	[46]
768	hydroxyl radical	proteins	
784	Cytosine and Uracil	DNA/RNA	[35]
798	O–P–O	Phospholipids/ carbohydrates	[44,47]
823	O-P-O DNA	DNA	[43,48]
878	O-O stretching of H_2O_2	Cell wall	[37]
929	ν(C-C), stretching-probably in amino acids proline & valine (protein band)	Proteins	[43]
959	C–C–N stretch	Proteins	[43]
1006	Methionine (SO, stretching)	Proteins	[43,49]
1032	O-P-O DNA	DNA	[36]
1054	C–O stretching, C–N stretching (protein)	Proteins	[35]
1103	Phenylalanine	Proteins	[45,46]
1158	C–C/C–N stretching	Lipids	[35]
1415	(=C–C) unsaturated fatty acids	Lipids	[35]
1191	Cytosine, guanine	DNA/RNA	[45,46]
1208	Amide III & CH_2 wagging vibrations from glycine backbone & proline side chains	Proteins	[43]
1208	Guanine	DNA	[43]
1239	Amide III	Proteins	[43,44]
1328	NH2 str (A, polyadenine and DNA), C˙H def	DNA/RNA, Protein	[45,46]
1415	=C–C= unsaturated fatty acids	Lipid	[35]
1460	CH_2	Lipids,Proteins	[35]
1469	Adenine and Guanine	DNA/RNA	[44]
1515	Cytosine	DNA/RNA	[45,46]
1604	Amide I	Proteins	[43]
1610	υ (C=C), Tryptophan	Proteins	[39]

samples as compared with ligand and unexposed/control fungal samples. The inhibition of β-1, 3-glucan synthase reduces the formation of cell wall carbohydrate patches and delays cell integrity failure and fungal death. It is proposed that the selenium complex in current study (azole complex) exert their fungicidal activity by inhibiting synthesis of cell wall carbohydrate patches, thereby killing the fungus [34].

The decrease in the intensities of SERS spectral features at 1415 cm^{-1} (=C–C=unsaturated fatty acids (lipid)) and 1460 cm^{-1} (CH_2 lipid) show decease in fungal lipid contents in complex and ligand exposed fungal samples as compared with unexposed/control sample. The lipids are the main components of fungal cell membrane and decarease in lipid contents is directly related with the destruction of fungal cell [35]. Similarly, a SERS spectral feature at 1032 cm^{-1} (O-P-O DNA) is directly relaed with enhanced rate of saturation of unsaturated fatty acids of fungal cell after its exposure with complex and ligand as compared with unexposed/control fungal sample [36]. A reduced intensity of SERS spectral feature at 878 $cm^{-1}$is due to O-O stretching of H_2O_2 in *A. niger* fungus in complex exposed fungal sample as compared with ligand and control fungal samples which is correlated with destruction of H_2O_2 molecules present in *A. niger* fungal sample [37].

Other two SERS spectral features of hydroxyl radicals at 768 cm^{-1} (hydroxyl radical) and 1281 cm^{-1} (hydroxyl radical) can confirmd the destruction of fungal H_2O_2 molecules. The hydroxyl radical is a type of reactive oxygen species (ROS) which causes oxidative stress inside fungal cell which in turn causes several intracellular damages [38]. The oxidative stress enhances some of the stress proteins which can be observed by reduction in the intensities of SERS features at 650 cm^{-1} (C–S stretch and C–C twist (Protein)), 1052 cm^{-1} (C-N stretching (protein)), 1208 cm^{-1} (Guanine), 1032 cm^{-1} (O-P-O DNA), 1420–1480 cm^{-1} (CH deformation mode (protein)), 1610 cm^{-1} (υ (C=C), Tryptophan) and 1208 cm^{-1} (C=O group of amino acid). [39].

The SERS feature at 630 cm^{-1} υ(O-C=O) of oxalic acid) is due to the oxidation of protein content (Glutamyl amino acid), which is related with denaturation and conformational changes of proteins in complex exposed fungal samples as compared with ligand and unexposed/control fungal samples [37]. The methionine is an important protein and another SERS feature at 1006 cm^{-1} is due to the oxidized form of methionine (S-O, stretching) which acts as a major chemical pathway for the degradation of protein molecules [40].The oxidative stress causes fungal DNA fragmentation which can be observed by SERS feature at 1191 cm^{-1} [41].

Fig. 2 shows SRES spectra of ligand exposed A. niger **(L2)**, complex exposed A.niger **(C2;** Zn-NHC complex**)** and control *A. niger*. The SERS spectral features which are arised due to biochemical changes inside the fungal cell after ligand and complex exposure as compared with unexposed/control include 592 cm^{-1} (υ(C–C–C) of cell wall component), 650 cm^{-1} (C–S stretch and C–C twist (Protein)), 674 cm^{-1} (ring breathing mode), 734 cm^{-1} (hypoxanthine), 784 cm^{-1} (nucleic acids (cytidine, uracil)), 823 cm^{-1} (O-P-O DNA), 765 cm^{-1} (O-P-O DNA), 878 cm^{-1} (O-O stretch (H_2O_2)), 929 cm^{-1} (R-CH_3 of valine), 959 cm^{-1} (C–C–N stretch (protein)), 1006 cm^{-1} (SO, stretching), 1032 cm^{-1} (O-P-O DNA), 1054 cm^{-1} (C-N stretching (protein)), 1103 cm^{-1} (Phenylalanine), 1156 cm^{-1} (O6-H1/C8-H8 rocking in hypoxanthine), 1181 cm^{-1} (Guanine radical), 1208 cm^{-1} (Guanine), 1239 cm^{-1} (Amide III and Amide I of proteins), 769 cm^{-1} (Hydroxyl radical), 1328 cm^{-1} (υ (NH_2) adenine, polyadenine, DNA), 1610 cm^{-1} (tryptophan), 734 cm^{-1} (hypoxanthine), 1415 cm^{-1} (=C–C= unsaturated fatty acids (lipid)),1460 cm^{-1} (CH_2 lipid), 1420–1480 cm^{-1} (CH deformation mode (protein)), 1469 cm^{-1} (Adenine and Guanine), 1515 cm^{-1} (Cytosine), 1604 cm^{-1} (Amide I).

The SERS spectral features which are directly related with DNA/RNA contents of fungal cell include 784 cm^{-1} (nucleic acids (cytidine, uracil)), 1328 cm^{-1} (υ (NH_2) adenine, polyadenine, DNA), 1469 cm^{-1} (Adenine and Guanine) and their intensities are continously decearing from ligand to complex as compared with unexposed/control. In case of Zn-NHC complex, only minor changes in the fungal cell wall components are observed at 1208 cm^{-1}, 1239 cm^{-1} and 1604 cm^{-1} due to change in protein composition. These changes in the intensity indicate possible changes in amide-III and glycine components which cause degradation in backone of protein structure.

3.1. Principal component analysis (PCA)

Principal component analysis (PCA) is used for differentiating the SERS spectral data of unexposed/control, complex exposed and ligand exposed *A. niger* fungus. PCA clearly differentiates these different SERS spectral data sets as shown in PCA scatter plot in Fig. 3.

Fig. 3**(a-i)** shows the PCA scatter plot of SERS spectral data sets of ligand exposed, Se-NHC complex (C1) exposed *A. niger* fungus samples (with red dots) versus unexposed/control *A. niger* fungus samples. The PC1 clearly differentiates three groups of spectra with explained variance (89.94 %) and PC2 explains the ramaining variabilty (8.46 %). To understand the basis of discrimination in the scatter plot, the loadings of PC1 are presented in Fig. 3**(a-ii)**.

The SERS spectral features on the positive side of loadings are related with Se-NHC complex (C1) exposed exposed fungal samples and SERS spectral features on the negative side of loadings are related with unexposed/control *A. niger* fungus samples. The SERS spectral features of

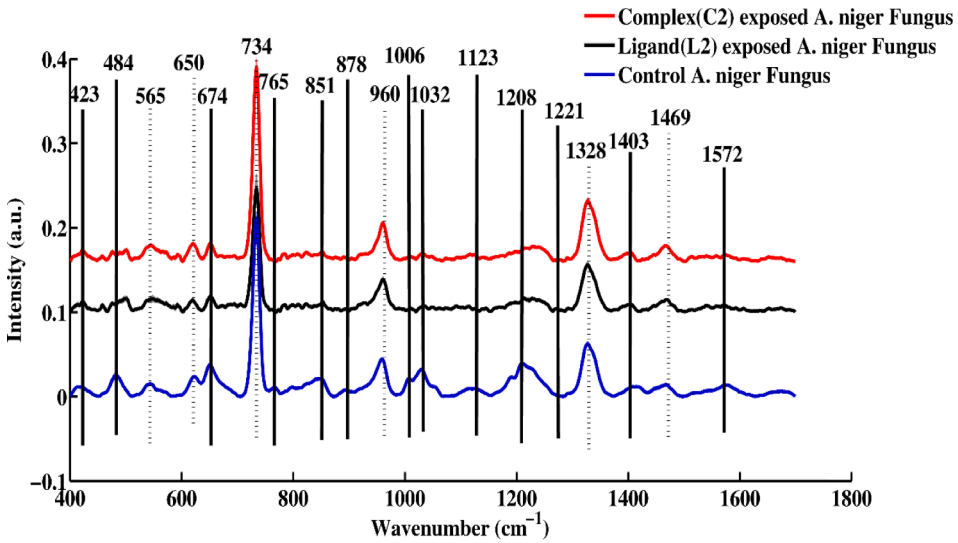

Fig. 2. The SRES spectra of ligand exposed A. niger **(L2)**, complex exposed A.niger **(C2)** and control *A. niger* **(C)**. SERS spectral data along with potenially differentiating features are labelled with solid and dotted lines and are listed in Table 1.

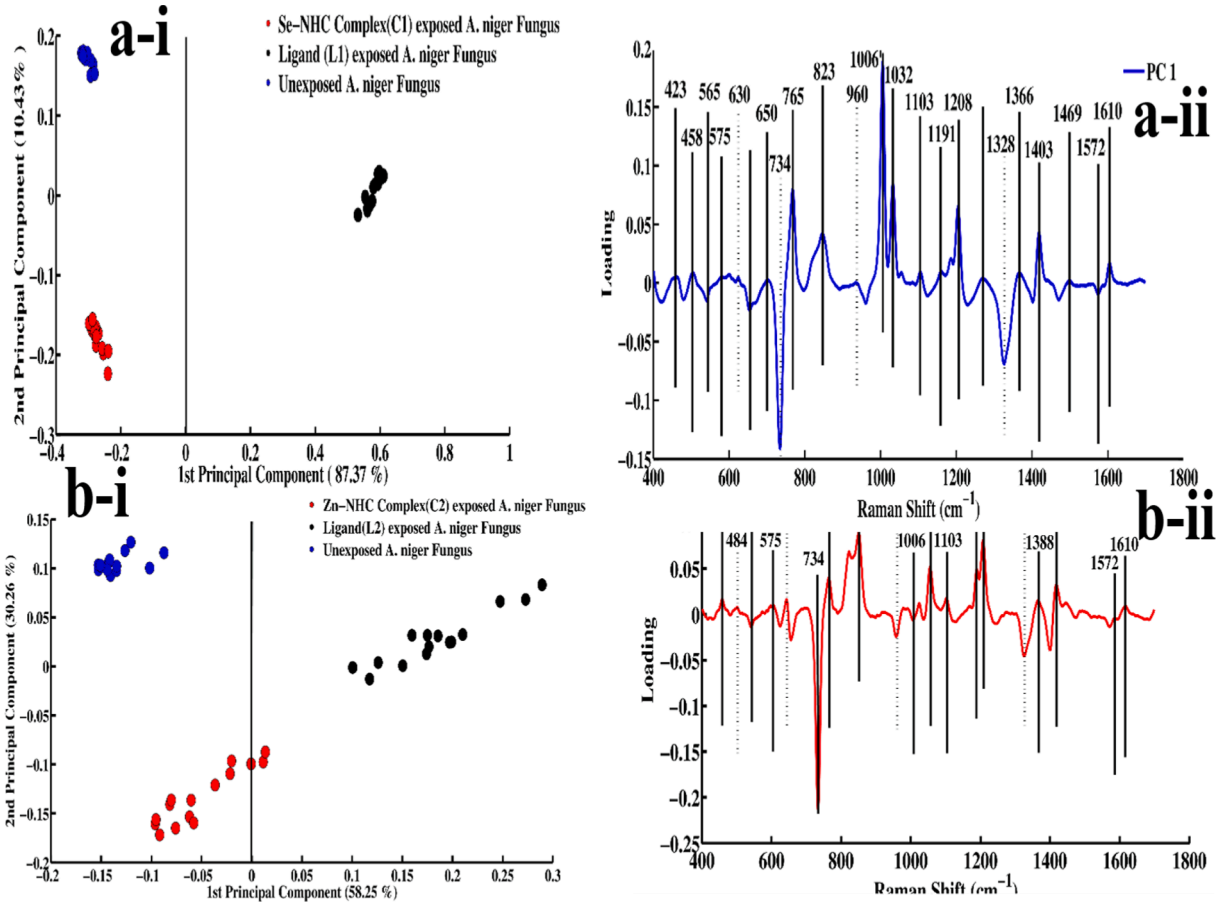

Fig. 3. PCA comparison between SERS spectral data of NHC comples exposed *A. niger* fungas and control *A. niger* fungus samples. **a(i)** PCA scatter plot of SERS spectral data of Se-NHC complex (C1) exposed *A. niger* fungus samples (red) versus control *A. niger* fungus samples (blue), **a(ii)** PCA loading of Se-NHC complex (C1) exposed *A. niger fungus* samples versus control *A. niger* fungus samples. **b(i)** PCA scatter plot of SERS spectral data of Zn-NHC complex (C2) exposed *A. niger* fungus samples (red) versus control *A. niger* fungus samples (blue), **b(ii)** PCA loading of Zn-NHC complex (C2) exposed *A. niger* fungus samples versus control *A. niger* fungus samples. (For interpretation of the references to colour in this figure legend, the reader is referred to the web version of this article.)

positive loadings include 565 cm^{-1} (υ(C-C-C) of cell wall component), 650 cm^{-1} (C–S stretch and C–C twist (Protein)), 575 cm^{-1} (Glycosidic ring mode), 734 cm^{-1} (hypoxanthine), 765 cm^{-1} (O-P-O DNA), 784 cm^{-1} (nucleic acids (cytidine, uracil)), 823 cm^{-1} (O-P-O DNA), 765 cm^{-1} (O-P-O DNA)), 878 cm^{-1} (O–O stretch H_2O_2), 929 cm^{-1} (R-CH_3 of valine), 959 cm^{-1} (C–C–N stretch (protein)), 1006 cm^{-1} (S–O,

stretching), 1032 cm^{-1} ((O-P-O DNA), 1054 cm^{-1} (C-N stretching (protein)), 1415 cm^{-1} (=C–C= unsaturated fatty acids (lipid)), 1191 cm^{-1} (Guanine radical), 1208 cm^{-1} (Guanine), 1239 cm^{-1} (Amide III and Amide I of proteins), 786 cm^{-1} (Hydroxyl radical), 1328 cm^{-1} (υ (NH_2) adenine, polyadenine, DNA), 1610 cm^{-1} (tryptophan), 1460 cm^{-1} (CH_2 lipid), 1420–1480 cm^{-1} (CH deformation mode (protein), 1469 cm^{-1} (Adenine and Guanine), 1515 cm^{-1} (Cytosine), 1103 cm^{-1} (Phenylalanine) and 1604 cm^{-1} (Amide I). Some SERS spectral features which are related with DNA/RNA contents of funguss include 784 cm^{-1} (nucleic acids (cytosine, uracil)), 786 cm^{-1} (C, T, U ring breathing), 1328 cm^{-1} (υ (NH_2) adenine, polyadenine, DNA), 1469 cm^{-1} (Adenine and Guanine) and their intensities are continously decearing from ligand to complex as compared with unexposed/control.

The SERS spectral features of negative loadings include 565 cm^{-1} (υ(C–C–C) of cell wall component), 575 cm^{-1} (Glycosidic ring mode), 734 cm^{-1} (hypoxanthine), 784 cm^{-1} (nucleic acids (cytosine, uracil)), 1158 cm^{-1} (C–C stretching in lipid), 1054 cm^{-1} (C-N stretching (protein)), 1415 cm^{-1} (=C–C= unsaturated fatty acids (lipid)), 1208 cm^{-1} (Guanine), 768 cm^{-1} (Hydroxyl radical), 1293 cm^{-1} (CH deformations (protein)), 1328 cm^{-1} (υ (NH_2) adenine, polyadenine, DNA), 1610 cm^{-1} (tryptophan), 1460 cm^{-1} (CH_2 lipid), 1420–1480 cm^{-1} (CH deformation mode (protein)) and 1469 cm^{-1} (Adenine and Guanine). These SERS spectral features are in correspondance with the SERS spectral features of mean plot as shown in Fig. 1**.**

Fig. 3(b-i) shows the PCA scatter plot of SERS spectral data sets of Zn-NHC complex (C2) exposed *A. niger* fungus samples with red dots versus unexposed/control *A. niger* fungus samples where PC1 explains variance of 58.25% and PC2 explains the ramaining variabilty (30.26%). To understand the basis of discrimination in the scatter plot, the loadings of PC1 are presented in Fig. 3**(b-ii)**. The SERS spectral features on the positive side of loadings are related with Complex(C2) exposed fungal samples and SERS spectral features on the negative side of loadings are related with unexposed/control *A. niger* fungus samples. The SERS spectral features of positive loadings include 565 cm^{-1} (υ(C–C–C) of cell wall component), 650 cm^{-1} (C–S stretch and C–C twist (Protein)), 575 cm^{-1} (Glycosidic ring mode), 734 cm^{-1} (hypoxanthine), 765 cm^{-1} (O-P-O DNA), 784 cm^{-1} (nucleic acids (cytidine, uracil)), 823 cm^{-1} (O-P-O DNA), 765 cm^{-1} (O-P-O DNA), 878 cm^{-1} (O–O stretch H_2O_2), 929 cm^{-1} (R-CH_3 of valine), 959 cm^{-1} (C–C–N stretch (protein)), 1006 cm^{-1} (S–O, stretching), 1032 cm^{-1} (O-P-O DNA), 1054 cm^{-1} (C-N stretching (protein)), 1415 cm^{-1} (=C–C= unsaturated fatty acids (lipid)), 1191 cm^{-1} (Guanine radical), 1208 cm^{-1} (Guanine), 1239 cm^{-1} (Amide III and Amide I of proteins), 786 cm^{-1} (Hydroxyl radical), 1328 cm^{-1} (υ (NH_2) adenine, polyadenine, DNA), 1610 cm^{-1} (tryptophan), 1460 cm^{-1} (CH_2 lipid), 1420–1480 cm^{-1} (CH deformation mode (protein)), 1469 cm^{-1} (Adenine and Guanine), 1515 cm^{-1} (Cytosine), 1103 cm^{-1} (Phenylalanine) and 1604 cm^{-1} (Amide I). Some SERS spectral features which are related with DNA/RNA contents of funguss include 784 cm^{-1} (nucleic acids (cytosine, uracil)), 786 cm^{-1} (C, T, U ring breathing), 1328 cm^{-1} (υ (NH_2) adenine, polyadenine, DNA), 1469 cm^{-1} (Adenine and Guanine) and their intensities are continously decearing from ligand to complex as compared with unexposed/control.

The SERS spectral features of negative loadings include 565 cm^{-1} (υ(C–C–C) of cell wall component), 575 cm^{-1} (Glycosidic ring mode), 734 cm^{-1} (hypoxanthine), 765 cm^{-1} (O-P-O DNA), 784 cm^{-1} (nucleic acids (cytosine, uracil)), 1158 cm^{-1} (C–C stretching in lipid), 1054 cm^{-1} (C-N stretching (protein)), 1415 cm^{-1} (=C–C= unsaturated fatty acids (lipid)), 1208 cm^{-1} (Guanine), 768 cm^{-1} (Hydroxyl radical), 1293 cm^{-1} (CH deformations (protein)), 1328 cm^{-1} (υ (NH_2) adenine, polyadenine, DNA), 1610 cm^{-1} (tryptophan), 1460 cm^{-1} (CH_2 lipid), 1420–1480 cm^{-1} (CH deformation mode (protein)) and 1469 cm^{-1} (Adenine and Guanine). These SERS spectral features are in correspondance with the SERS spectral features of mean plot as shown in Fig. 2**.**

The comparison of the loadings of PCA, Fig. 3(a-ii) and (b-ii) indicastes that the PCA loadings which are only present as changes in the Se-complex exposeed *A.Niger* (Fig. 3 (a-ii)) and absent in the Zinc-complex exposeed *A.Niger* (Fig. 3 (a-ii)) include 765 cm^{-1} (O-P-O DNA), 823 cm^{-1} (O-P-O DNA), 1032 cm^{-1} (O-P-O DNA), 1208 cm^{-1} (Guanine). This can lead to conclude that Se-complex exposeed causes biochemical changes in *A.Niger* through DNA damage but Zinc-complex exposeed *A. Niger* involves changes in the peaks related to proteins hence causes damage throughfungal cell wall. This can help to elucidate the differentiation of modes of action of both the complexes against *A.Niger*. Moreover, Comparison between Mean SRES difference spectra of Zn-NHC complex and Se-NHC complex exposed A. niger with control *A. niger*, is presented in the supplementary material as **Fig. S-2**.

3.2. Partial least squares discriminant analysis (PLS-DA)

The PLS-DA is a classification model that was performed for the differentiation of SERS spectral data sets of *A. niger* fungus exposed to Se-NHC complex and Zn-NHC. The data of all the complexes and unexposed/control *A. niger* fungus was randomized and independently split into 45% training data-set (60 spectra) and 55% test data-set (60 spectra). The Montecarlo cross-validation was employed with PLS-DA based on the Bayes theorem. The optimal number of components or latent variables (OptLVs) were extracted based on the lowest prediction error that gives the highest accuracy in results. In the present study, 18 OptLVs were chosen by cross-validation to train the classification model. The original variables were projected to obtain the cross validated **y**-predicted scores from this model that have been shown in Fig. 4.

The antifungal activity of Se-NHC complex and Zn-NHC complexes is differentiated with 99.8% sensitivity, 100% specificity and 100% accuracy. Furthermore, the receiver operating characteristic (ROC) curve also shows the efficiency of the PLS-DA classification model classification potential of SERS as shown in Fig. 4**(d)**. The ROC curve has been plotted between the true classification (sensitivity) and false classification (specificity). The area under ROC curve was 0.82 that indicates the excellent performance of the model because it is close to 1.

The inhibition of growth in *Aspergillus niger* fungus upon exposure to NHCs complexes is associated with the effect of deficiency of proteins and decomposition of cell wall components. The β-1,3-glycosidic linkage in carbohydrates is hydrolyzed by NHCs complexes. The exposure of complexes to fungus can change the cell wall components such as lipopolysaccharide and membrane proteins. These changes in the cell wall components and fungal DNA/RNA leads to the changes in the SERS spectral fingerprints of *Aspergillus niger* fungus. The SERS bands which may belong to the fungus are identified and confirmed by finding their consistent appearance as unique features by individually comparing all the Se-NHCs and Zn-NHCs complexes as compared to unexposed/ control *Aspergillus niger*.

All fungal strains belong to the same specie (A. niger) due to which the major peak positions of all complexes exposed fungal samples are identical but there are many marked differences among typical SERS vibrational bands and their relative intensities at 575 cm^{-1}, 565 cm^{-1}, 624 cm^{-1}, 650 cm^{-1}, 765 cm^{-1}, 784 cm^{-1}, 823 cm^{-1}, 893 cm^{-1}, 1004 cm^{-1}, 1032 cm^{-1}, 1123 cm^{-1}, 1208 cm^{-1} and 1415 cm^{-1}. The intensity of the band at 734 cm^{-1} and 1328 cm^{-1} are increased in Se-NHCs complex exposed fungus that shows the increased content of adenine and polyadenine of DNA in them which indicates the presence of plasmid (DNA) for the enhanced DNA contents observed. The band at 823 cm^{-1} (O-P-O DNA) is absent in unexposed/control fungus that shows the loss of outer membrane porins in them and the band at 543 cm^{-1} ($C^{-}C^{-}C$) in-plane bending in carbohydrates) is also absent in them. These spectral features are clearly disappeared in the Zn-NHC complex exposed *A. niger* fungus showing that these complexes are effective as antifungal agents. The major limitations of the proposed method are size of nanoparticles because the diverse size range of nanoparticles and requirement of a skilled person for using Matlab software for the SERS spectral data preprocessing and analysis. Therefore, in the present study Authors have used narrow range of nanoparticles in order to avoid the shortcomings of applied method [50,51].

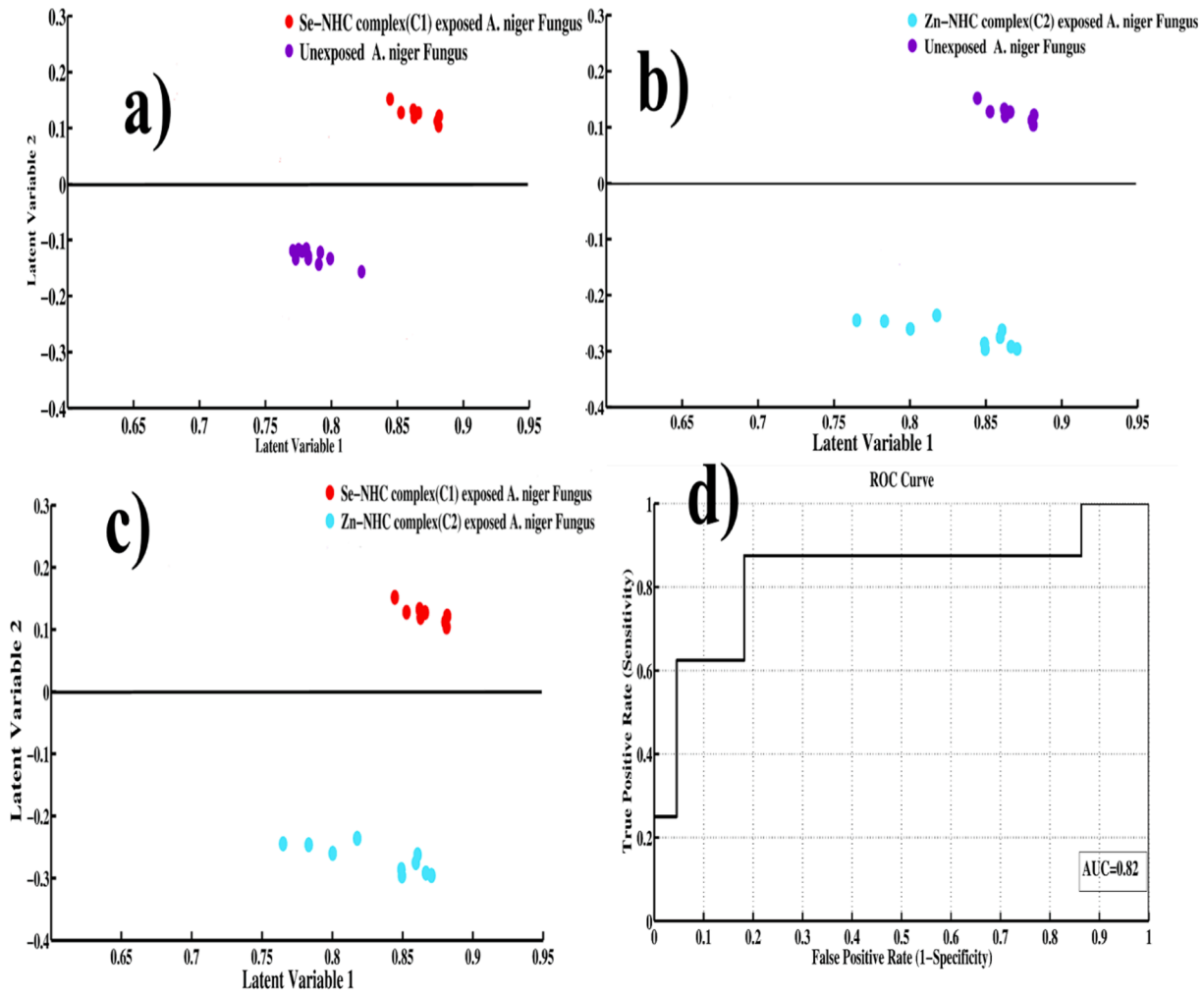

Fig. 4. **(a)** PLS-DA scatter diagram of SERS spectral data of Se-NHC complex (C1) exposed *A. niger* fungus (red)) versus control *A. niger* fungus (Purple) **(b)** Zn-NHC complex (C2) exposed *A. niger* fungus (magneta) versus control *A. niger* fungus (Purple) **(c))** PLS-DA scatter diagram of SERS spectral data of Se-NHC complex (C1) exposed *A. niger* fungus (red)) versus Zn-NHC complex (C2) exposed *A. niger* fungus (magneta) **(d)** Reciever operating characteristic curve (ROC) showing area under curve (AUC). (For interpretation of the references to colour in this figure legend, the reader is referred to the web version of this article.)

4. Conclusions

The mortality rate due to fungal infections has been increasing due to resistance of fungal pathogens against antifungal drugs. Novel organometallic complexes provide antifungal activity against fungus by inhibiting its growth. Surface enhanced Raman spectroscopy provides a rapid and non-destructive analysis to differentiate spectral data sets of different samples of *Aspergillus niger* fungal samples exposed to NHC complexes due to biochemical changes in cell wall. SERS technique has a potential to differentiate the mechanism of action of Se-NHC complexes and Zn-NHC complexes against *Aspergillus niger* fungus. The SERS spectral features obtained upon exposure of NHC organometallic complexes show the biochemical changes in the protein and cell wall components as a result of inhibition of growth. The principal component analysis of SERS spectral data sets obtained is utilized to check the variability in spectral of fungus exposed to Se-NHC and Zn-NHC complexes. PLS-DA is also employed to classify these groups of spectral data of *Aspergillus niger* fungus with 99.8% sensitivity, 100% specificity and 100% accuracy.

CRediT authorship contribution statement

Ali Raza: Writing – original draft. **Soneya Parveen:** Writing – review & editing. **Muhammad Irfan Majeed:** Supervision. **Haq Nawaz:** Project administration. **Muhammad Rizwan Javed:** Resources. **Muhammad Adnan Iqbal:** Resources. **Nosheen Rashid:** Validation. **Muhammad Zeeshan Haider:** Data curation. **Muhammad Zeeshan Ali:** Software. **Amina Sabir:** Software. **Hafiz Mahmood ul Hasan:** Formal analysis. **Beenish Majeed:** Formal analysis.

Declaration of Competing Interest

The authors declare that they have no known competing financial interests or personal relationships that could have appeared to influence the work reported in this paper.

Acknowledgments

This research did not receive any specific grant from funding agencies in the public, commercial, or not-for-profit sectors.

Appendix A. Supplementary material

Supplementary data to this article can be found online at https://doi.org/10.1016/j.saa.2022.121903.

References

[1] C. Mota Fernandes, et al., The future of antifungal drug therapy: novel compounds and targets, Antimicrob. Agents Chemother. 65 (2) (2021) e01719–20.
[2] A. Chakrabarti, et al., Fungal rhinosinusitis: a categorization and definitional schema addressing current controversies, The Laryngoscope 119 (9) (2009) 1809–1818.
[3] M.I. Hutchings, A.W. Truman, B. Wilkinson, Antibiotics: past, present and future, Curr. Opin. Microbiol. 51 (2019) 72–80.
[4] F. Nazzaro, et al., Essential oils and antifungal activity, Pharmaceuticals 10 (4) (2017) 86.
[5] M. Patra, G. Gasser, N. Metzler-Nolte, Small organometallic compounds as antibacterial agents, Dalton Trans. 41 (21) (2012) 6350–6358.
[6] S.A. Patil, et al., N-heterocyclic carbene metal complexes as bio-organometallic antimicrobial and anticancer drugs, Future Med. Chem. 7 (10) (2015) 1305–1333.
[7] N. Wang, et al., Supplementation of micronutrient selenium in metabolic diseases: its role as an antioxidant. Oxidative Medicine and Cellular Longevity, 2017.
[8] L. Kuršvietienė, et al., Selenium anticancer properties and impact on cellular redox status, Antioxidants 9 (1) (2020) 80.
[9] F. Bisceglie, et al., Antibacterial activity of metal complexes based on cinnamaldehyde thiosemicarbazone analogues, J. Inorg. Biochem. 203 (2020) 110888.
[10] S.H. Sumrra, et al., A review on the efficacy and medicinal applications of metal-based triazole derivatives, J. Coord. Chem. 73 (20–22) (2020) 2838–2877.
[11] W. Ahmad, et al., Synthesis of selenium–silver nanostructures with enhanced antibacterial, photocatalytic and antioxidant activities, Appl. Nanosci. 10 (4) (2020) 1191–1204.
[12] G.B. Alvi, et al., Biogenic selenium nanoparticles (SeNPs) from citrus fruit have anti-bacterial activities, Sci. Rep. 11 (1) (2021) 1–11.
[13] N. Zhou, et al., Research progress on the biological activities of selenium polysaccharides, Food Funct. 11 (6) (2020) 4834–4852.
[14] K. Shanker, et al., Ru (II) complexes of N4 and N2O2 macrocyclic Schiff base ligands: Their antibacterial and antifungal studies, Spectrochim. Acta Part A Mol. Biomol. Spectrosc. 73 (1) (2009) 205–211.
[15] D. Menezes, et al., The in vitro antifungal activity of some dithiocarbamate organotin (IV) compounds on Candida albicans—a model for biological interaction of organotin complexes, Appl. Organomet. Chem. 22 (4) (2008) 221–226.
[16] J. Bajwa, et al., Quantitative analysis of solid dosage forms of cefixime using Raman spectroscopy, Spectrochim. Acta Part A Mol. Biomol. Spectrosc. 238 (2020) 118446.
[17] H. Nawaz, et al., Evaluation of the potential of Raman microspectroscopy for prediction of chemotherapeutic response to cisplatin in lung adenocarcinoma, Analyst 135 (12) (2010) 3070–3076.
[18] K. Scherlach, K. Graupner, C. Hertweck, Molecular bacteria-fungi interactions: effects on environment, food, and medicine, Annu. Rev. Microbiol. 67 (2013) 375–397.
[19] J. Kneipp, Nanosensors based on SERS for applications in living cells, in: Surface-Enhanced Raman Scattering, Springer, 2006, pp. 335–349.
[20] M. Arabi, et al., Label-free SERS detection of Raman-inactive protein biomarkers by Raman reporter indicator: toward ultrasensitivity and universality, Biosens. Bioelectron. 174 (2021) 112825.
[21] M. Arabi, et al., Molecular imprinting: green perspectives and strategies, Adv. Mater. 33 (30) (2021) 2100543.
[22] M. Arabi, L. Chen, Technical challenges of molecular-imprinting-based optical sensors for environmental pollutants, Langmuir (2022).
[23] S. Schlücker, Surface-Enhanced raman spectroscopy: concepts and chemical applications, Angew. Chem. Int. Ed. 53 (19) (2014) 4756–4795.
[24] J. Wang, et al., A nanoplasmonic label-free surface-enhanced Raman scattering strategy for non-invasive cancer genetic subtyping in patient samples, Nanoscale 9 (10) (2017) 3496–3503.
[25] H. Fang, et al., Ultrasensitive and quantitative detection of paraquat on fruits skins via surface-enhanced Raman spectroscopy, Sens. Actuat., B 213 (2015) 452–456.
[26] K. Loza, et al., The dissolution and biological effects of silver nanoparticles in biological media, J. Mater. Chem. B 2 (12) (2014) 1634–1643.
[27] N. Leopold, et al., The role of adatoms in chloride-activated colloidal silver nanoparticles for surface-enhanced Raman scattering enhancement, Beilstein J. Nanotechnol. 9 (1) (2018) 2236–2247.
[28] H. Nawaz, et al., Prediction of viral loads for diagnosis of Hepatitis C infection in human plasma samples using Raman spectroscopy coupled with partial least squares regression analysis, J. Raman Spectrosc. 48 (5) (2017) 697–704.
[29] R.N. Cassar, et al., Synthesis of size tunable monodispersed silver nanoparticles and the effect of size on SERS enhancement, Vib. Spectrosc. 71 (2014) 41–46.
[30] S. Bashir, et al., Surface-enhanced Raman spectroscopy for the identification of tigecycline-resistant *E. coli* strains, Spectrochim. Acta Part A Mol. Biomol. Spectrosc. 258 (2021) 119831.
[31] M. Kashif, et al., Surface-enhanced Raman spectroscopy for identification of food processing bacteria, Spectrochim. Acta Part A Mol. Biomol. Spectrosc. 261 (2021) 119989.
[32] Z. Guo, et al., Label-free surface enhanced Raman scattering spectroscopy for discrimination and detection of dominant apple spoilage fungus, Int. J. Food Microbiol. 338 (2021) 108990.
[33] I. Clemente, M. Aznar, C. Nerin, Raman imaging spectroscopy as a tool to investigate the cell damage on Aspergillus ochraceus caused by an antimicrobial packaging containing benzyl isothiocyanate, Anal. Chem. 88 (9) (2016) 4772–4779.
[34] B. Geißel, et al., Azole-induced cell wall carbohydrate patches kill Aspergillus fumigatus, Nat. Commun. 9 (1) (2018) 1–13.
[35] L. He, et al., Antifungal activity of zinc oxide nanoparticles against Botrytis cinerea and Penicillium expansum, Microbiol. Res. 166 (3) (2011) 207–215.
[36] H. Noothalapati, et al., Label-free chemical imaging of fungal spore walls by Raman microscopy and multivariate curve resolution analysis, Sci. Rep. 6 (1) (2016) 1–10.
[37] E. Cabiscol Català, J. Tamarit Sumalla, J. Ros Salvador, Oxidative stress in bacteria and protein damage by reactive oxygen species, Int. Microbiol. 3(1) (2000) 3–8.
[38] Y. Hong, et al., Post-stress bacterial cell death mediated by reactive oxygen species, Proc. Natl. Acad. Sci. 116 (20) (2019) 10064–10071.
[39] M.B. Angelova, et al., Oxidative stress response of filamentous fungi induced by hydrogen peroxide and paraquat, Mycol. Res. 109 (2) (2005) 150–158.
[40] B. Sjöberg, et al., Methionine oxidation by hydrogen peroxide in peptides and proteins: a theoretical and Raman spectroscopy study, J. Photochem. Photobiol., B 188 (2018) 95–99.
[41] J. Choi, et al., Proton transfer of guanine radical cations studied by time-resolved resonance Raman spectroscopy combined with pulse radiolysis, J. Phys. Chem. Lett. 6 (24) (2015) 5045–5050.
[42] M. Mathlouthi, D.V. Luu, Laser-raman spectra of d-glucose and sucrose in aqueous solution, Carbohydr. Res. 81 (2) (1980) 203–212.
[43] E. Witkowska, et al., Detection and identification of human fungal pathogens using surface-enhanced Raman spectroscopy and principal component analysis, Anal. Methods 8 (48) (2016) 8427–8434.
[44] F. Huang, et al., Membrane damage mechanism contributes to inhibition of trans-cinnamaldehyde on Penicillium italicum using Surface-Enhanced Raman Spectroscopy (SERS), Sci. Rep. 9 (1) (2019) 1–10.
[45] C. Wang, et al., Photophoretic trapping-Raman spectroscopy for single pollens and fungal spores trapped in air, J. Quant. Spectrosc. Radiat. Transfer 153 (2015) 4–12.
[46] S. Stöckel, et al., The application of Raman spectroscopy for the detection and identification of microorganisms, J. Raman Spectrosc. 47 (1) (2016) 89–109.
[47] I. Sayin, et al., Characterization of yeast species using surface-enhanced Raman scattering, Appl. Spectrosc. 63 (11) (2009) 1276–1282.
[48] Z. Huang, et al., Near-infrared Raman spectroscopy for optical diagnosis of lung cancer, Int. J. Cancer 107 (6) (2003) 1047–1052.
[49] O. Samek, et al., Candida parapsilosis biofilm identification by Raman spectroscopy, Int. J. Mol. Sci. 15 (12) (2014) 23924–23935.
[50] A. Mushtaq, et al., Surface-enhanced Raman spectroscopy (SERS) for monitoring colistin-resistant and susceptible *E. coli* strains, Spectrochim. Acta Part A Mol. Biomol. Spectrosc. 278 (2022) 121315.
[51] C. Farber, et al., Advanced spectroscopic techniques for plant disease diagnostics. A review, TrAC, Trends Anal. Chem. 118 (2019) 43–49.